The human placenta dictates the phenotype of decidual macrophages.

Sigrid Vondra[1], Anna-Lena Höbler[1], Andreas Ian Lackner[1], Johanna Raffetseder[2], Zala Nikita Mihalic[3], Leila Saleh[4], Victoria Kunihs[4], Peter Haslinger[1], Markus Wahrmann[5], Heinrich Husslein[6], Raimund Oberle[7], Julia Kargl[3], Sandra Haider[4], Paulina Latos[8], Martin Knöfler[4], Jan Ernerudh[9], Jürgen Pollheimer[1]*

[1]Department of Obstetrics and Gynecology, Reproductive Biology Unit, Maternal-fetal Immunology Group, Medical University of Vienna, Austria; [2]Division of Inflammation and Infection (II), Department of Biomedical and Clinical Sciences (BKV), Linköping University, Linköping, Sweden. [3]Otto Loewi Research Center, Division of Pharmacology, Medical University of Graz, Austria. [4]Department of Obstetrics and Gynecology, Reproductive Biology Unit, Placental Development Group, Medical University of Vienna, Austria; [5]Division of Nephrology and Dialysis, Department of Medicine III, Medical University of Vienna, Vienna, Austria; [6]Department of Obstetrics and Gynecology, Medical University of Vienna, Vienna, Austria; [7]Center for Pathobiochemistry and Genetics, Institute of Medical Chemistry, Medical University of Vienna, Austria; [8]Center for Anatomy and Cell Biology, Medical University of Vienna, A-1090 Vienna, Austria [9]Department of Clinical Immunology and Transfusion Medicine, Department of Biomedical and Clinical Sciences, Linköping University, Linköping, Sweden.

Short title: The placenta induces decidual macrophages

* Correspondence to Jürgen Pollheimer: juergen.pollheimer@muv.ac.at

Abstract

During human pregnancy, placenta-derived extravillous trophoblasts (EVT) invade the decidua and communicate with maternal immune cells. The decidua can be distinguished into basalis (decB) and parietalis (decP), the latter being unaffected by placentation. By defining a novel gating strategy, we report accumulation of myeloid cells in decB. We identified a decidua basalis-associated macrophage (decBAM) population with a differential transcriptome and secretome when compared to decidua parietalis-associated macrophages (decPAMs). decBAMs are CD11c^{hi} and efficient inducers of Tregs, proliferate *in situ* and secrete high levels of CXCL1, CXCL5, M-CSF, and IL-10. In contrast, decPAMs exert a dendritic cell-like, motile phenotype characterized by induced expression of HLA class II molecules, enhanced phagocytosis, and the ability to activate T cells. Strikingly, EVT-conditioned media are able to convert decPAMs into a decBAM phenotype. Cumulatively, these findings assign distinct macrophage phenotypes to decidual areas depending on placentation and further highlight a critical role for EVTs in the induction of pregnancy-tolerant macrophage polarization.

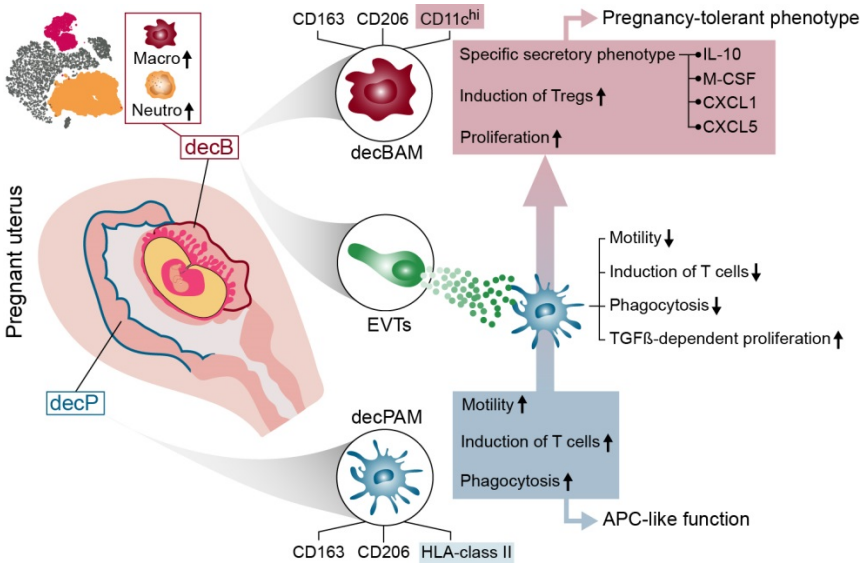

In this study we identified so far unrecognized, placenta-dictated immune responses at the maternal-fetal interface. Altogether we imply that placenta-derived trophoblasts induce a pregnancy-tolerant phenotype by suppressing antigen presenting cell-like functions in maternal tissue macrophages.

49 **Introduction**

50 During human pregnancy, fetal-derived placental extravillous trophoblasts (EVTs) invade the
51 decidualized mucosal uterine surface, referred to as decidua (1). This unique process, in
52 which semi-allogeneic EVTs intermingle and communicate with maternal decidual immune
53 cells, is fundamental for the maintenance and success of pregnancy. An imbalance in these
54 interactions can lead to the development of obstetrical syndromes such as preeclampsia or
55 uterine growth restriction (2). The human decidua has been the subject of various studies
56 directed towards understanding the function of uterine immune cell types. In order to enable
57 fetal tolerance, the maternal-fetal interface is dominated by a non-cytotoxic immune cell
58 response, which supports placental function (3, 4). A central role in the maintenance of this
59 tissue-specific, pregnancy-sustaining environment has been assigned to an interactive
60 network between EVTs and maternal immune cells. Remarkably, decidual natural killer
61 (dNK) cells and macrophages cooperate to transform the decidual vasculature into dilated
62 conduits able to deliver high amounts of low-pressure blood to the growing fetus (5). The
63 pivotal role of decidual immunology in pregnancy has further been underlined by
64 demonstrating a pregnancy-specific memory in dNK cells with the ability to support
65 reproductive success (6). Moreover, there are also indications for an active suppression of
66 immune responses at the maternal-fetal interface. In humans, EVTs have been
67 demonstrated to induce a non-cytotoxic phenotype in dNK cells by initiating intercellular
68 trafficking of the non-classical MHC-I class molecule HLA-G (7). In addition, studies in mice
69 suggest an active blockage of T cell infiltration at the maternal-fetal interface even after
70 forced reactivation of maternal memory T cells by placenta-specific overexpression of
71 ovalbumin (8). However, little is known about the specific function of decidual macrophages.
72 A recent paper identified various maternal macrophage subpopulations in the human
73 decidua, two of which constitute tissue resident cells, referred to as dM1 and dM2, and one is
74 found in the intervillous space adhering to placental villi, designated as dM3 (9). The dM3
75 type was recently characterized and identified as placenta-associated maternal
76 macrophages (PAMMs) (10). In this paper, the authors also unraveled distinctive phenotypes

77 of fetal-derived placental macrophages, referred to as Hofbauer cells (HB). Different to HBs
78 and PAMMs in the intervillous space, decidual tissue-resident macrophages are not
79 uniformly confronted with placental tissues. During early pregnancy, placentation takes place
80 only at a rather distinctive uterine site, the decidua basalis (decB), whereas large areas of
81 the decidua, the decidua parietalis (decP), are unaffected by placentation. While various
82 morphological differences such as degree of vascularization (11, 12) or tissue stiffness (13)
83 have been noticed, little is known about the difference between decB and decP tissues in
84 terms of immune cell content and activation. In a recent publication, we were able to show
85 low abundance of T cells in decB tissues when compared to decP samples. The drop in both
86 $CD4^+$ helper and $CD8^+$ cytotoxic T cells was further associated with low abundance of T cell-
87 recruiting high endothelial venules (12). These findings imply fundamental differences in
88 immune cell distribution and extravasation into decB and decP. However, to date, there are
89 no comparative data on immune cell distribution or function in decB and decP tissues that
90 allow conclusions to be drawn about placentation-dependent effects on decidual immune
91 cells.
92 In this study, we set out to select donor-matched first-trimester decB and decP tissue
93 samples in order to identify immunological adaptation that specifically occur in response to
94 placentation. By defining a novel flow cytometry gating strategy, we demonstrate that tissue-
95 resident macrophages and neutrophils accumulate in decB tissues. We further identified a
96 specific phenotype and functionality of decB-associated macrophages (decBAMs) in
97 comparison to decP-associated macrophages (decPAMs). While decBAMs show a higher
98 capacity to proliferate and induce Treg formation, decPAMs are more motile and phagocytic,
99 and efficiently induce T cell proliferation.
100
101

Results

Myeloid cells specifically accumulate at the maternal-fetal interface

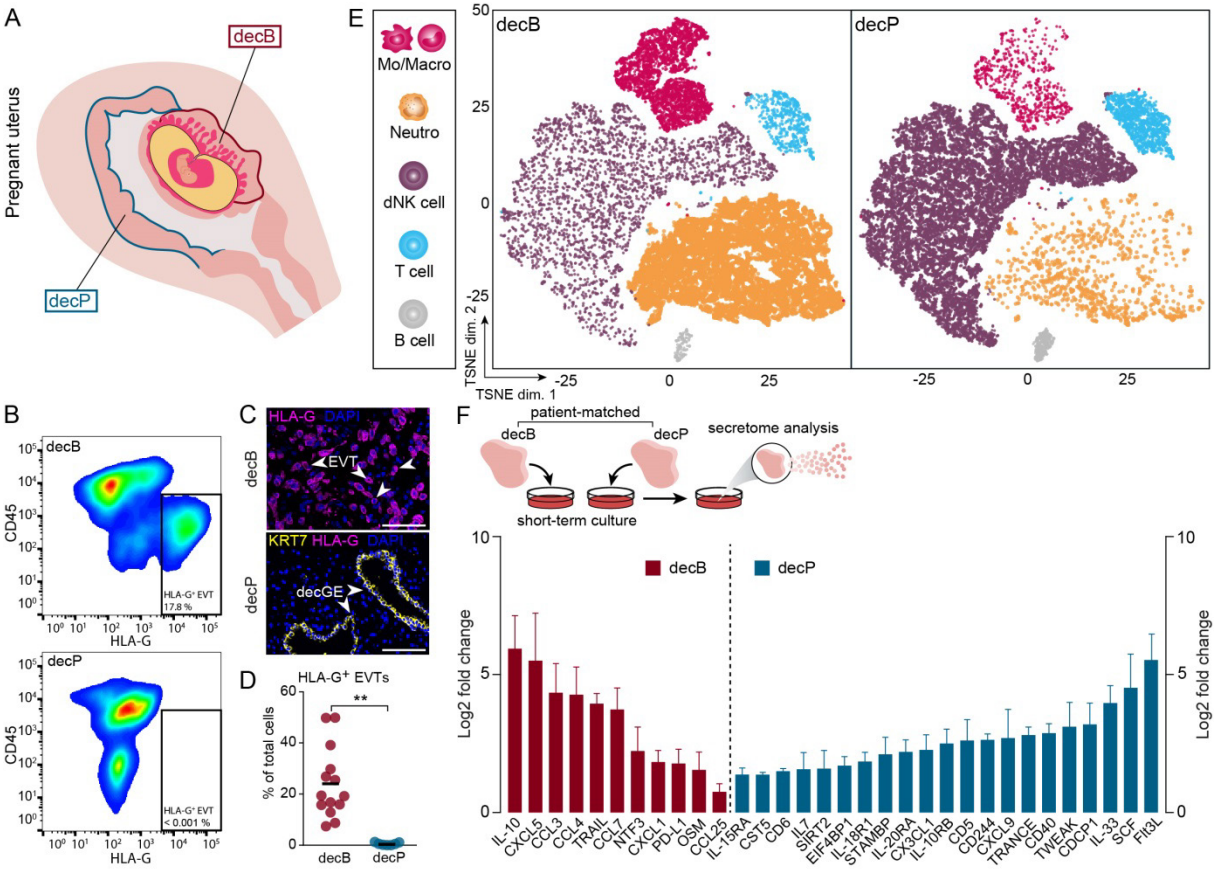

Figure 1.**Investigation of immune cell distributions in first-trimester decidual samples identifies myeloid cell accumulation in first-trimester decB tissues. (A)** Schematic drawing of a human pregnant uterus during the first trimester of pregnancy indicating decidua basalis (encircled by a red line, decB) and decidua parietalis (encircled by a blue line, decP). **(B)** Representative flow cytometry plots of decB and decP tissue cell isolates demonstrating distribution of CD45$^+$ immune cells and HLA-G$^+$ EVTs. The percentages of HLA-G$^+$ EVTs are indicated. **(C)** IF stainings of first-trimester decidual tissue sections showing HLA-G (magenta) and DAPI (blue) in the upper section and keratin 7 (KRT7; yellow), HLA-G (magenta) and DAPI (blue) in the lower tissue section. Representative images of *n* = 25 experiments. Scale bar, 100 µm. **(D)** Quantification of HLA-G$^+$ EVTs in first-trimester decB (n = 14) and decP (n = 7) cell isolates, analyzed by Student's t-test. The center line represents the mean. **(E)** TSNE plot showing distribution of major immune cell populations in decB and decP created from flow cytometry data of patient-matched tissue samples **(F)** Summary data (log2 fold change, n = 4) for the significant differences in secreted factors from patient-matched decB and decP tissue explants after 20 h in culture measured by the proximity extension assay (www.Olink.com). The schematic drawing shown on the top illustrates the experimental set-up. Data are represented as mean + SD (standard deviation). Significances were calculated using multiple t-tests. **, P ≤ 0.01. decGE, decidual glandular epithelium; EVT, extravillous trophoblast; Mo/Macro, monocytes, macrophages; Neutro, neutrophils; dNK cell, decidual natural killer cell.

In this study, we aimed at identifying placentation-specific immune modulation in the human decidua during early human pregnancy. To this end, we established a cohort of first-trimester decidual samples including areas affected by placentation (decidua basalis, decB) and donor-matched areas that do not interact with villous placental tissues (decidua parietalis, decP) (Fig. 1A). The presence of EVTs and abundance of glandular epithelium served as

127 markers to separate decB from decP (Fig. 1, B and C), respectively. An overview of our
128 tissue sampling strategy is outlined in Fig. S1, A and B. Overall, we found that cell isolates
129 from first-trimester decB tissues contain on average 22 % of HLA-G^{+} EVTs compared with <
130 0.001 % ($3.24*10^{-3}$) of EVTs in decP tissues (Fig. 1 D) and that the total cellular density is
131 significantly lower in decB when compared to matched decP samples (Fig. S1 C). Next, we
132 defined the distribution of the major immune cell subtypes in decB and decP tissues,
133 revealing an accumulation of myeloid CD45^{+}CD14^{+} monocytes/macrophages and
134 CD45^{+}CD66b^{+} neutrophils in decB samples (Fig. 1 E).
135 With the exception of a few studies, decidual infiltration with neutrophils is a poorly described
136 phenomenon. This is likely because most protocols used to determine decidual immune cell
137 populations by flow cytometry include neutrophil-depleting density centrifugation. Well in line,
138 comparative analyses of secreted factors from decB and decP tissue explants revealed an
139 overrepresented myeloid-associated cytokine signature in decB tissues, including IL-10,
140 CXCL1, CCL3, CCL4, CXCL5, and suppressors of T cell immunity (TRAIL and PD-L1). In
141 contrast, decP samples showed elevated levels of factors involved in T cell, DC, and NK cell
142 immunity such as IL-7, CXCL1, sCD5, sCD6, TRANCE or Flt3 (Fig. 1 F).
143
144 **Formation of decB is associated with the accumulation of tissue-resident**
145 **macrophages**
146 To further increase the resolution of our data we applied specific markers to dissect
147 macrophages from infiltrating blood monocytes. *In situ* dual immunofluorescence (IF) staining
148 confirmed that all CD14^{+} cells residing in the decidual stroma also express the pan
149 macrophage marker CD68 and in addition are uniformly positive for CD163 and CD206 (Fig.
150 S2 A). Subsequent flow cytometry analysis of decidual cell isolates revealed two CD14^{+}
151 populations, one lacking CD163 and CD206 expression and the other highly positive for both
152 tissue macrophage markers (Fig. 2 A). While the latter CD163^{+}CD206^{+} population showed a
153 typical enlarged cell size and morphology with abundant vacuoles as well as high
154 autofluorescence, as is commonly observed in macrophages (14), CD14^{+}CD163^{-}CD206^{-}
155 cells displayed a morphology typical for monocytes such as smaller cell size or little

granularity (Fig. 2, B and C). Bulk RNA-seq confirmed this notion by demonstrating that CD14$^+$CD163$^+$CD206$^+$ cells express typical hallmark genes of tissue-resident macrophages such as *MERTK*, *CD68*, *MAFB* or *FCGR2A* (15) and express comparatively low levels of monocyte marker genes including L-selectin (*SELL*), *S100A12*, *S100A8*, and *S100A9* (Fig. 2 D and Fig. S2 C). Indeed, IF-analysis shows that CD14$^+$S100A12$^+$ monocytes are found in the lumen of decidual vessels and not in the tissue stroma (Fig. S2 B).

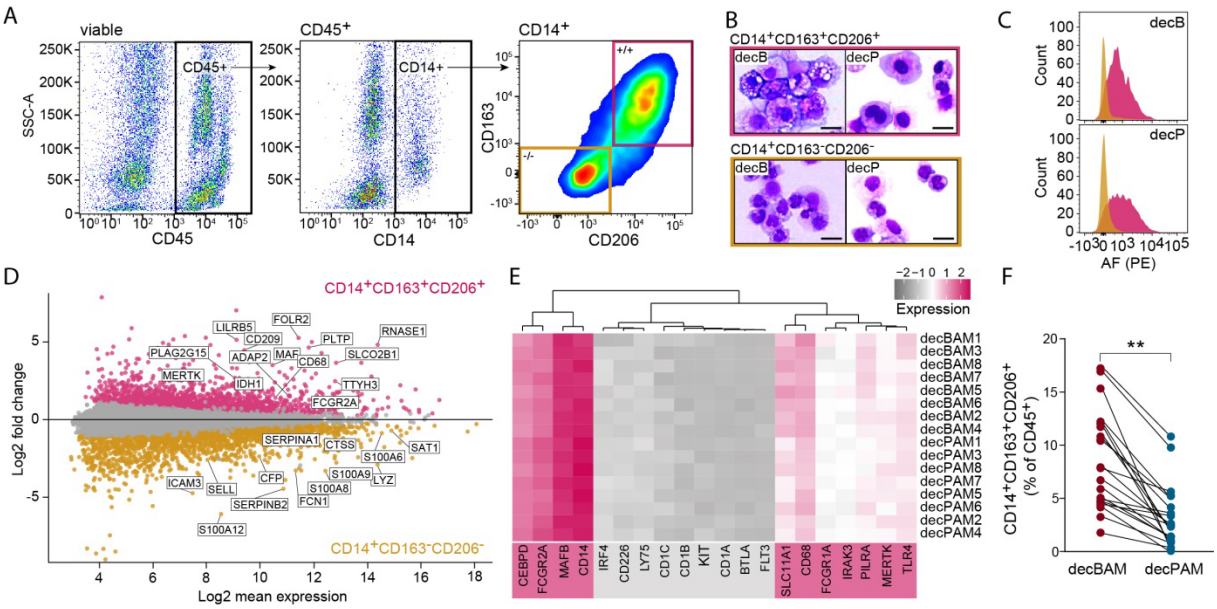

Figure 2. **Isolation and characterization of tissue-resident decidual macrophages (A)** Flow cytometry gating strategy used to identify tissue-resident decidual macrophages by a CD45$^+$CD14$^+$CD163$^+$CD206$^+$ expression profile. Pink gate, CD14$^+$CD163$^+$CD206$^+$ macrophages. Orange gate, CD14$^+$CD163$^-$CD206$^-$ monocytes. **(B)** Macrophage (pink rectangle) and monocytic (orange rectangle) populations from decB and decP were sorted and stained by Giemsa staining. Representative images of *n* = 4 experiments. Scale bar, 20 µm. **(C)** Representative flow cytometry plots identifying autofluorescence (AF) in isolated CD14$^+$CD163$^+$CD206$^+$ (pink histogram) and CD14$^+$CD163$^-$CD206$^-$ (orange histogram) cell isolates from decB and decP. **(D)** MA plot of differentially expressed genes (DEGs) from RNA-seq. Pink and orange dots represent significantly up- or down-regulated DEGs in isolated CD14$^+$CD163$^+$CD206$^+$ (n = 8 pairs) and CD14$^+$CD163$^-$CD206$^-$ (n = 4 pairs) cells from decB and decP tissues. **(E)** Heatmap showing expression of macrophage (underlaid with pink)- and DC (underlaid with grey)-associated hallmark genes in isolated decBAM and decPAM. **(F)** Dotplot demonstrating distribution of CD14$^+$CD163$^+$CD206$^+$ decBAMs and decPAMs in patient-matched first-trimester decB and decP samples (n = 21 pairs). Patient-matched samples are indicated via connected dot plots. P-value was generated using paired t-test. **, P ≤ 0.01. decB, decidua basalis; decP, decidua parietalis; decBAM, decB-associated macrophage; decPAM, decP-associated macrophage.

Next, we analyzed whether our isolated decidual macrophage populations may express DC core markers retrieved from various hallmark papers deciphering macrophage and DC signature gene expression in human and mice (14, 16, 17). As expected, decidual macrophages express conserved lineage markers such as *MERTK* and *MAFB* as well as other typical markers for human and mouse macrophages, including *CD14*, *CD68*, *CEBPD*, *FCGR1A* (CD64) or *FCGR2A* (CD32). In contrast, DC-associated lineage markers such as

185 *CD1A*/*B*/*C*, *CD226*, *FLT3* or *KIT* were absent from both populations (Fig. 2 E). By
186 considering our established markers for tissue-residency we were able to show a decB-
187 associated accumulation of tissue macrophages (Fig. 2 F). Moreover, comparative studies
188 with non-pregnant uterine samples associate the pregnancy-specific rise in dNK cells with
189 decP and highlights accumulation of myeloid cells as a placentation-dependent event at the
190 maternal-fetal interface (Fig. S2 D). Finally, we termed macrophages obtained from different
191 decidual compartments decBAMs and decPAMs, respectively.
192 These data show that placentation is associated with increased numbers of true tissue-
193 resident macrophages.
194
195 **Accumulation of decidual tissue macrophages is associated with *in situ* proliferation**
196 We next sought to determine the potential of decB to recruit neutrophils and macrophages.
197 Therefore, we generated conditioned media (CM) from cultivated patient-matched decB and
198 decP tissue samples and performed chemoattractant assays using isolated PBMCs or
199 neutrophils from peripheral blood samples. These assays revealed no differential effect
200 between decB- and decP-CM in the recruitment of $CD14^+$ blood-derived monocytes (Fig. 3 A)
201 or other PBMCs, including T cell subtypes, B cells or NK cells (Fig. 3 A, Fig. S3 A). In
202 contrast, separate assays showed that decB-CM exert a significantly higher potential to
203 attract blood neutrophils (Fig. 3 B). Well in line, culture media of decB tissues contained high
204 levels of well-described neutrophil chemoattractants including CXCL1, CXCL8, S100A8, and
205 S100A9 (18, 19) (Fig. 3 C). Strikingly, *in situ* IF staining showed significantly more
206 $CD14^+Ki67^+$ macrophages in decB tissues when compared with decP sections (Fig. 3 D).
207 Decidual tissue macrophages also expressed a wide array of cell cycle markers including
208 CCNA1, pRB, and CDK1 (Fig. 3 E). In addition, we observed the presence of mitotic figures
209 in tissue-resident $CD14^+$ decidual macrophages (Fig. 3 E). Finally, an *ex vivo* proliferation
210 assay determining EdU incorporation into cultivated decidual explants revealed that
211 decBAMs are capable of *de novo* DNA synthesis, again to a greater extent than decPAMs
212 (Fig. 3 F).

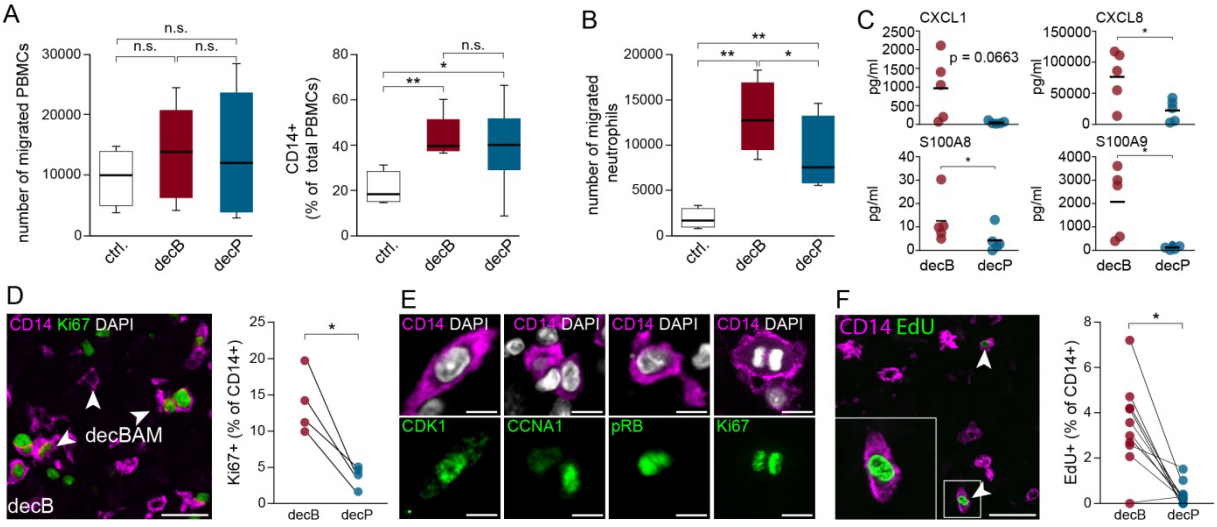

Figure 3. **decB-associated accumulation of myeloid cells is accomplished by chemoattractant factors and local proliferation of decBAMs (A)** Migratory response of PBMCs (left diagram) and $CD14^+$ blood cells (right diagram) to culture medium containing decB- or decP-CM (1:4, n = 8). Decidua culture medium was used as a control. P-values were generated using Repeated-measures ANOVA with Tukey's multiple comparison test. **(B)** Migratory response of blood neutrophils to culture medium without or with decB- and decP-CM (1:2, n = 4). Boxes in box plots represent upper and lower quartiles. The center line represents the median. Whiskers show the minimum and maximum of the data. P-values were generated using Repeated-measures ANOVA with Tukey's multiple comparison test. **(C)** Secretory profile of cultivated (20 hours), patient-matched decB and decP explants (n = 5 pairs) measured by bead-based multiplex immunoassays. Dots show measured levels in pg/ml. The center line represents the mean. P-values were generated using paired t-tests. **(D)** Representative IF staining of a first-trimester decB tissue section showing CD14 (magenta) and Ki67 co-staining (green). Quantification of four patient-matched decB and decP tissue samples is shown to the right by a dot plot. Each dot represents the percentage of $Ki67^+CD14^+$ double-positive cells for each tissue sample (n = 4 pairs). Scale bar, 20 µm. Patient-matched samples are shown in connected dot plots. P-value was generated using a paired t-test. **(E)** IF co-staining of first-trimester decB tissue sections showing cell cycle markers including CDK1, CCNA1, pRB in green and CD14 in magenta. The two images to the right upper and lower panel demonstrate a Ki67 expressing mitotic figure in a $CD14^+$ cell. DAPI (white) was used to visualize nuclei. Scale bars, 2 µm. **(F)** Representative IF staining of a cultivated decB explant tissue demonstrating EdU (green) incorporation into $CD14^+$ (magenta) macrophages, indicated by arrowheads. Inset picture shows a EdU+ macrophage at higher magnification. Quantification of EdU incorporation into $CD14^+$ macrophages of cultivated decB and decP first-trimester tissue explants. Each dot represents the percentage of $CD14^+$ EdU^+ cells for each tissue sample evaluated (n = 10 pairs). Patient-matched samples are indicated via connected dot plots. Scale bar, 20 µm. P-value was generated using a paired t-test. *, P ≤ 0.05; **, P ≤ 0.01, n.s.: not significant. decB, decidua basalis; decP, decidua parietalis.

These results suggest that decB-specific accumulation of tissue macrophages is driven by *in situ* proliferation and that, as expected, neutrophils are specifically recruited from blood.

decBAMs show a distinctive transcriptional and secretory phenotype

In-depth analysis of our bulk RNA-seq-based transcriptome data revealed substantial differences between isolated patient-matched decBAMs and decPAMs, which are shown to form two distinct groups by principal component analysis (PCA) (Fig. S4 A). We identified 1127 significantly differentially expressed genes (DEGs, adjusted p value < 0.05) between decBAMs (512 up) and decPAMs (615 up) (Fig. 4 A). Immune-related DEGs included *ITGAX*

248 (CD11c), *CD44*, *CXCL2*, and *ANPEP* in decBAMs, and *AXL*, *GAS6*, *SELENOP*, *C3*, and
249 *IL2RA* in decPAMs (Fig. 4 A). IF- and flow cytometry-based analyses confirmed higher
250 expression of HMOX1, CD44, and CD11c protein in decBAMs (Fig. 4 B). Moreover,
251 functional gene enrichment analysis revealed that gene sets involved in
252 granulocyte/neutrophil activation and myeloid immune responses were overrepresented in
253 decBAM-associated DEGs (Fig. S4 B). Prior to our study, three tissue-resident myeloid cell
254 types have been identified by single-cell (sc) RNA-seq, designated as decidual macrophage
255 1 (dM1), decidual macrophage 2 (dM2) and dendritic cell 1 (DC1) (9). A third decidual
256 macrophage subtype (dM3) identified in this study, later defined as a subtype of placenta-
257 associated maternal macrophages (PAMMs), does not constitute a decidua-resident cell type
258 but is found in the intervillous blood space, adhering to placental villi (10). Our comparative
259 computational approach showed that transcripts upregulated in decPAMs clearly associated
260 with the dM2 phenotype whereas decBAMs showed a strong overlap with the previously
261 identified dM1-associated genes both in global and single gene expression pattern (Fig. 4 D).
262 Well in line, decBAM- or decPAM-associated DEGs identified by our bulk RNA-seq analysis
263 were also differentially regulated in dM1 and dM2 populations (Fig. 4 E). In addition,
264 decBAMs showed a closer similarity with dM3-specific signatures, compared to decPAM
265 (Fig. S4 C). To this end, we isolated PAMMs and confirmed their transcriptional overlap with
266 dM3 signatures but also with maternal blood-derived immune cells such as monocytes or
267 dendritic cells (DC2) (Fig. S 4 C). Overall, these data confirm that PAMMs originate from
268 different entities including blood monocytes and decidual macrophages (10). Next, we
269 digested decB and decP tissues in order to study the secretome of isolated and short-term
270 cultivated EVTs, neutrophils, decBAMs, and decPAMs (Fig. 4 F). All cells were sorted by
271 FACS except for EVTs, which were isolated via magnetic beads conjugated with anti-HLA-G.
272 Due to their large size, EVTs are very sensitive to the high pressure and shear forces in a
273 cell sorter and show improved viability when sorted over magnetic columns. Viability and
274 purity of EVTs were confirmed by flow cytometry after isolation (Fig. S4 D).

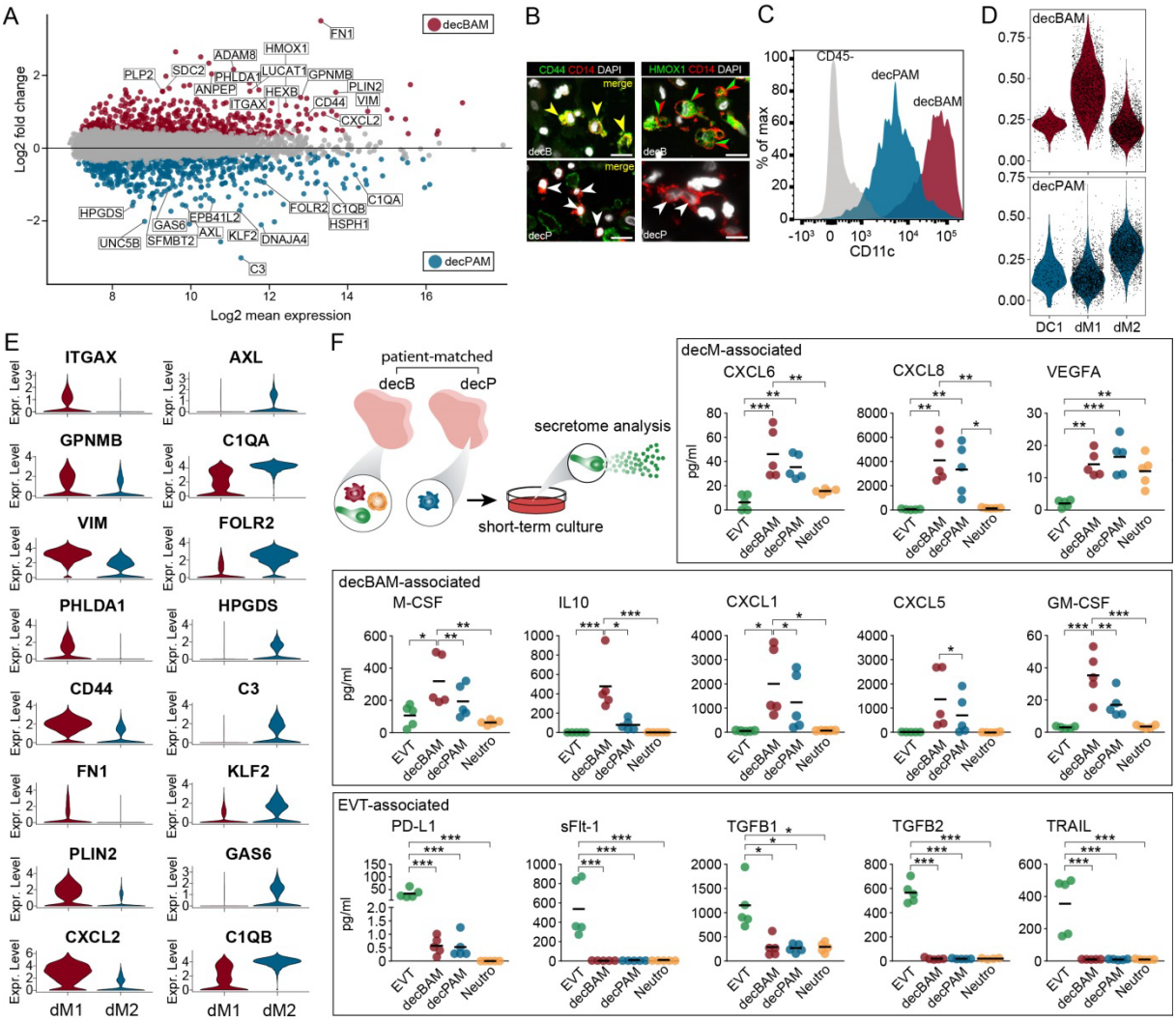

Figure 4. **First-trimester decBAMs and decPAMs differ in their transcriptional and secretory profile (A)** MA plot of DEGs from RNA-seq. Red and blue dots represent significantly up- or down-regulated DEGs in patient-matched isolated $CD14^{+}CD163^{+}CD206^{+}$ decBAMs and decPAMs (n = 8 pairs). **(B)** Representative IF co-staining of a first-trimester paraffin-embedded decB and decP tissue section showing HMOX1 and CD44 expression (green) in $CD14^{+}$ tissue macrophages (red). Arrowheads in yellow (left) or in green and red (right) indicate double positive cells. Scale bars, 20 µm. **(C)** Representative flow cytometric analysis of isolated decBAMs and decPAMs showing CD11c expression. **(D)** Violin plots showing expression of decBAMs (red) and decPAMs (blue) signatures in selected scRNA-seq clusters (Vento-Tormo et al., 2018). **(E)** Violin plots presenting expression of selected decBAM- and decPAM-associated gene transcripts in dM1 and dM2 scRNA-seq clusters (Vento-Tormo et al., 2018). **(F)** Secretory profile of magnetically sorted and cultivated (20 h) EVTs, decBAMs, decPAMS and neutrophils, determined by bead-based multiplex immunoassays (n = 5 pairs). Measured levels (pg/ml) of growth factors, chemokines and cytokines are shown as dots and the group mean is shown as centered line. The schematic drawing shown on the top illustrates the experimental set-up. P-values were generated using One-way ANOVA with Tukey's multiple comparison test. *, $P \leq 0.05$; **, $P \leq 0.01$; ***, $P \leq 0.001$. decB, decidua basalis; decP, decidua parietalis; decM, decidual macrophage; decBAM, decB-associated macrophage; decPAM, decP-associated macrophage; EVT, extravillous trophoblast; Neutro, neutrophil.

We determined secretion of cytokines and growth factors, which were selected based on our previous analyses and their involvement in myeloid or neutrophil immunity and function. In parallel, we measured these factors in decB and decP tissue explant CMs to control for a possible loss of tissue specificity upon single cell culture (Fig. S4 E). While decBAMs culture media contained significantly higher levels of CXCL1, CXCL5, GM-CSF, M-CSF, and IL-10,

298 decBAMs and decPAMs were equally efficient in releasing CXCL6, as well as high levels of
299 CXCL8. Among the macrophage-associated factors, the measured GM-CSF levels were the
300 lowest. All three immune cell populations secreted low but significantly induced levels of
301 VEGFA, when compared to EVTs. Our analyses further revealed that EVTs are efficient
302 producers of sPD-L1, TGFβ1, TGFβ2 and TRAIL. As a control for cell identity and
303 differentiation, we additionally analyzed EVT-specific sFlt-1 (20) (Fig. 4 F). Well in line, EVT-,
304 neutrophil-, and decBAM-associated factors were also significantly enriched in decB-CM with
305 the exception of M-CSF, GM-CSF and CXCL1, the latter showing elevated but not
306 significantly increased values (Fig. S4 E). Lastly, neutrophils secreted significantly higher
307 amounts of S100A8, S100A9, and MMP9 (Fig. S4 F).
308 In summary, decBAMs differ substantially from decPAMs by a specific transcriptome and
309 secretome.
310

311 **decBAMs induce Tregs and are suppressed in their APC-like function**

312 Our IF analyses show a strong difference in decBAM and decPAM appearance, the latter
313 exhibiting a more dendritic cell-like morphology (Fig. 5 A). Higher magnification clearly shows
314 an enhanced spindle-shaped morphology and formation of pseudopodia in decPAMs,
315 implying a more motile phenotype (Fig. 5 A). Interestingly, CD11c^{lo} decPAMs also showed a
316 more prominent staining with antibody against HLA class II molecules (Fig. 5 B). Well in line,
317 decPAMs transcripts are associated with significantly higher levels of *HLA-DOA*, *HLA-DPA1*
318 as well as *HLA-DRB1* and tended to show higher but not significantly elevated levels of *HLA-*
319 *DRA* (Fig. 5 C). To test whether decPAMs indeed show pronounced antigen presenting cell
320 (APC)-like functions we isolated decBAMs and decPAMs from the same donors and
321 performed functional *in vitro* assays. Comparative video-based analysis of freshly isolated
322 decidual macrophages indeed showed that decPAMs (Video 1) moved significantly faster
323 than decBAMs (Video 2) when tracked in real time (Fig. 5, D and E). In addition, decPAMs
324 also showed a significantly higher phagocytic activity when compared to decBAMs (Fig. 5, F

and G). A recent study suggests that decidual macrophages are efficient inducers of Treg formation (21).

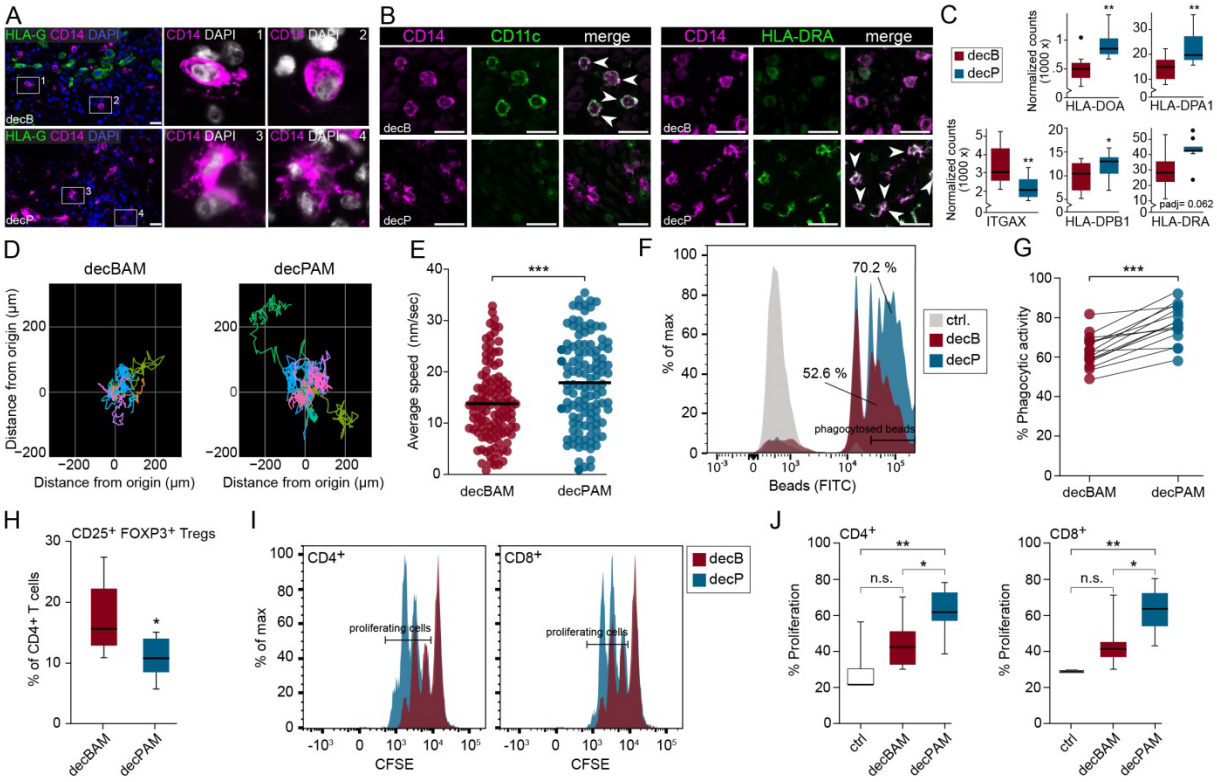

Figure 5. **decBAMs show a pregnancy-tolerating phenotype by suppressed APC-like function and enhanced ability to induce Treg formation. (A)** Representative IF staining of decB and decP tissue sections with antibodies against HLA-G (green) and CD14 (magenta). Zoomed insets on the right show appearance of $CD14^+$ macrophages in areas invaded by HLA-G^+ EVTs (1, 2) and those unaffected by placentation (3, 4). Representative images of *n* = 25 experiments. Scale bar, 20 µm. **(B)** IF co-stainings of first-trimester paraffin-embedded decB and decP tissue sections showing CD11c (green, left panel), HLA-DRA (green, right panel) and CD14 (magenta). White arrowheads indicate double positive cells. Representative images of *n* = 4 experiments. Scale bar, 50 µm **(C)** Box plots show normalized transcript levels of ITGAX and HLA class II molecules in FACS-sorted $CD14^+CD163^+CD206^+$ decBAMs and decPAMs analyzed by bulk RNA-seq (n = 8 pairs). Outliers are shown as dots and defined as data points outside 1.5 times the interquartile range above the upper quartile and below the lower quartile. P-values were calculated according to the recommended DESeq2 workflow. **(D)** Representative cell tracks of isolated and short-term (24 h) cultivated decBAMs and decPAMs were generated by live-cell microscopy (capture rate = 12 frames/h). Cell tracks were color-coded for each monitored cell over 12 h. **(E)** Dots present average speed of captured individual cell tracks (n = 117) of decBAMs and decPAMs cultures (n = 8 pairs). 7 outliers were removed by Grubbs' test. The center line represents the mean. P-value was generated using Student's t-test. **(F)** Representative flow cytometric analysis of phagocytosed FITC-labeled beads by decBAMs and decPAMs after 2 h of incubation. **(G)** Dots represent the percentage of phagocytosed FITC-labeled beads of each individual experiment performed (n = 15 pairs). Patient-matched samples are indicated via connected dot plots. P-value was generated using a paired t-test. **(H)** Box plots show the potential of decBAMs and decPAMs to induce $CD4^+FOXP3^+CD25^+$ Tregs from isolated $CD3^+$ blood T cells (n = 5). P-value was generated using paired t-test. **(I)** Representative flow cytometry plots showing CFSE dilution in $CD4^+$ and $CD8^+$ isolated blood T cells stimulated with anti-CD3/CD28 in the presence of decBAMs (red histogram) or decPAMs (blue histogram). **(J)** Box plots represent the median level of the percentage of dividing $CD4^+$ and $CD8^+$ T cells (at least one cell division as defined by CSFE dilution) in the absence or presence of decBAMs and decPAMs (n = 8). Box plots represent median values ± SEM. Boxes in box plots represent upper and lower quartiles. The center line represents the median. Whiskers show the minimum and maximum of the data. DAPI was used to visualize nuclei. P-values were generated using one-way ANOVA with Tukey's multiple comparison test. *, $P \leq 0.05$; **, $P \leq 0.01$; ***, $P \leq 0.001$. decB, decidua basalis; decP, decidua parietalis; decBAM, decB-associated macrophages; decPAM, decP-associated macrophages; Tregs, regulatory T cells.

By studying this phenomenon, we found that induction of $CD4^+CD25^+FOXP3^+$ Tregs is not a uniform feature of decidual macrophages since Treg induction was in particular executed by

361 decBAMs (Fig. 5 H). To further test for dendritic cell-like function, we studied the potential of
362 decidual macrophages to activate blood-derived T cells. To this end, we cultivated T cells
363 from healthy donors with decBAMs or decPAMs in a ratio of 10:1. In line with our previous
364 results, mainly decPAMs are able to trigger proliferation in both $CD4^+$ helper T cells and
365 $CD8^+$ cytotoxic T cells (Fig. 5, I and J).
366 Altogether, we show that decBAM are impaired in their ability to migrate, phagocytose, and
367 promote T cell proliferation but are efficient inducers of Tregs.
368

369 **The secretome of EVTs induces a decBAM-like phenotype**

370 Since our secretome screen of isolated EVTs revealed high secretion of immunomodulatory
371 factors (Fig. 4 F) we assumed that EVTs can alter decidual macrophage activation and
372 function. In order to avoid preconditioning by a decB environment likely under the control of
373 EVTs, we decided to test this by studying EVT-dependent effects on either whole decP
374 tissue explants or isolated decPAMs. To this end, we treated isolated decP tissue explants
375 with EVT-conditioned media (EVT-CM) and investigated possible alterations in decPAMs
376 upon treatment (Fig. 6 A). Immunofluorescence-based analysis indeed showed that addition
377 of EVT-CM significantly increases CD44 expression of decPAMs *in situ* to a comparable
378 level as detected in decB tissue explants (Fig. 6 B). Next, we exposed isolated decPAMs to
379 50% EVT-CM and found a significantly reduced motility and phagocytic activity (Fig. 6, C and
380 D). EVTs secrete high levels of the immunomodulatory factors TGFβ1 and TGFβ2, well
381 studied for their pleiotropic effects on macrophages, as well as high levels of PD-L1, which
382 has recently been suggested to inhibit macrophage phagocytosis when expressed by tumor
383 cells (22). However, the suppressive activity of EVT-CM towards the phagocytic activity of
384 decPAMs was not reversed by the addition of any of the blocking antibodies against TGFβ or
385 PD-L1 (Fig. 6 E). Next, we investigated the effect of EVT-CM on the ability of decPAMs to
386 interfere with T cell immunity. While neither EVT-CM alone nor in combination with decPAMs
387 affected Treg differentiation (Fig. S5 A), we found a significantly reduced decPAM-dependent
388 activation of $CD4^+$ and $CD8^+$ T cells upon treatment with EVT-CM (Fig. 6, F and G).

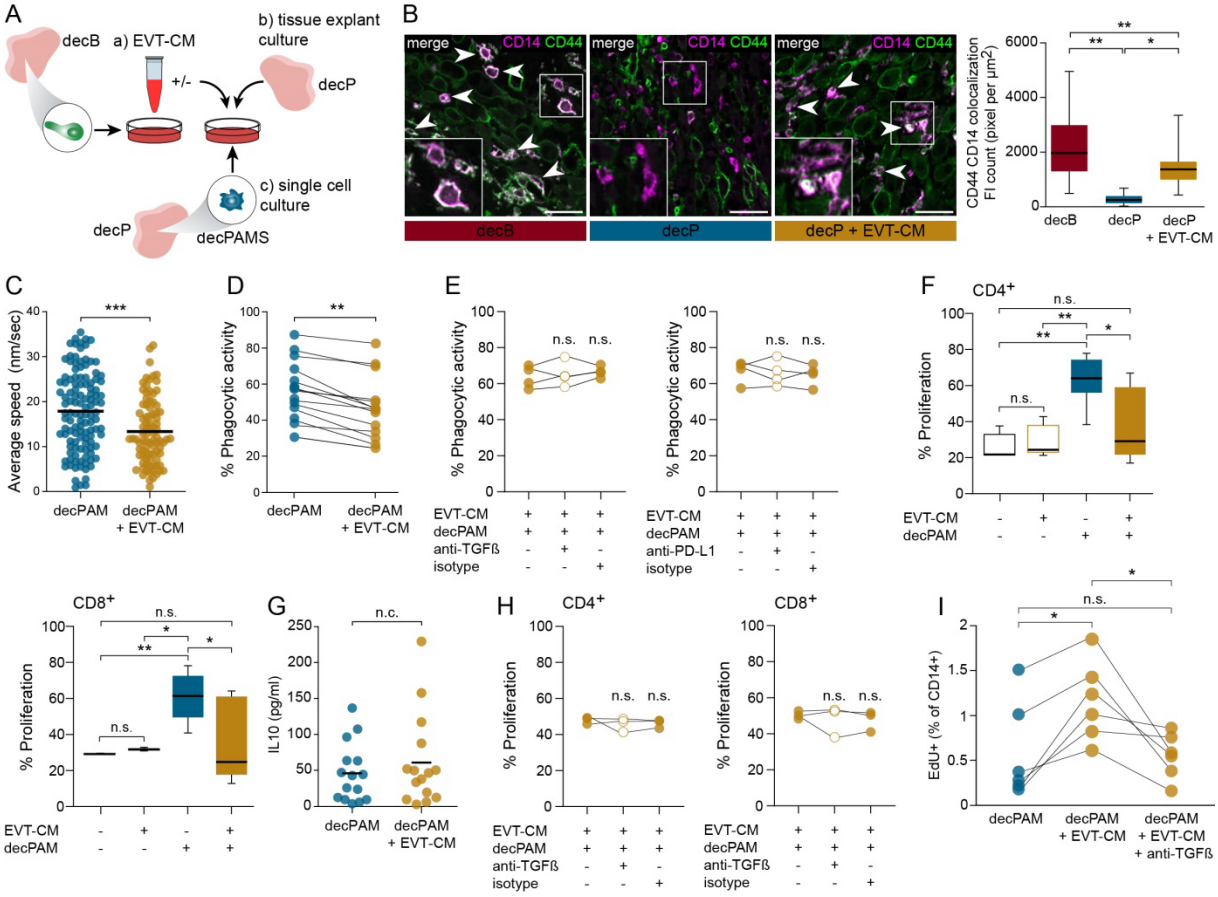

Figure 6. **decPAMs are functionally reprogrammed by the secretome of EVTs (A)** Schematic drawing to illustrate the experimental set up. EVTs were isolated by magnetic beads conjugated with anti-HLA-G and cultivated for 20 h to generate EVT-CM (a) used to stimulate decP tissue explants (b) or FACS-isolated decPAMs (c). **(B)** Representative double IF stainings using antibodies against CD14 (magenta) and CD44 (green) investigating overlapping CD14 CD44 expression in unstimulated decB and decP tissue cultures and EVT-CM stimulated decP explant cultures. Examples of overlapping signals are marked by white arrow heads. Box plots indicate median value of white pixels per μm^2 (generated by overlays of green and magenta colored CD14/CD44 co-stainings). P-values were generated using one-way ANOVA with Tukey's multiple comparison test. Scale bars, 20 µm **(C)** Diagram shows average speed of each cell tracked (n = 90) in independent experiments using isolated decPAMs either without or with stimulation with 50% EVT-CM (n = 6 pairs). 7 outliers were removed by Grubbs' test. The center line represents the mean. P-values was generated using a paired t-test. **(D)** Dot plot represents the percentage of phagocytosed FITC-labeled beads of each individual experiment performed (n = 14 pairs). Patient-matched samples are indicated via connected dot plots. P-value was generated using a paired t-test. **(E)** Phagocytosis assays were performed in the presence of EVT-CM alone, with isotype control or blocking antibodies for TGFβ or PD-L1. **(F)** Box plots show the percentage of proliferative $CD4^+$ or $CD8^+$ T cells stimulated with anti-CD3/CD28 in the absence or presence of decPAMs and/or EVT-CM (n = 7). P-values were generated using one-way ANOVA with Tukey's multiple comparison test. **(G)** Potential of short-term (20 h) cultivated decPAMs to secrete IL-10 (pg/ml) stimulated without or with EVT-CM (n = 15 pairs). **(H)** Box plots represent the percentage of dividing $CD4^+$ and $CD8^+$ T cells (at least one cell division as defined by CSFE dilution) stimulated with decPAMs and EVT-CM in the absence or presence of isotype control or a blocking antibody for TGFβ (n = 3). P-values were generated using one-way ANOVA with Tukey's multiple comparison test. **(I)** Percentage of EdU^+ nuclei in $CD14^+$ macrophages of cultivated decP first-trimester tissue explants. Each dot represents the percentage for each tissue sample evaluated (n = 6 pairs). Patient-matched samples are indicated via connected dot plots. P-values were generated using Repeated-measures ANOVA with Tukey's multiple comparison test. Boxes in box plots represent upper and lower quartiles. The center line represents the median. Whiskers show the minimum and maximum of the data. *, $P \leq 0.05$; **, $P \leq 0.01$; ***, $P \leq 0.001$, n.s.: not significant. decB, decidua basalis; decP, decidua parietalis; decBAM, decB-associated macrophages; decPAM, decP-associated macrophages; EVT-CM, extravillous trophoblast-conditioned medium.

Given that EVT-CM alone did not suppress $CD4^+$ or $CD8^+$ T cell proliferation (Fig. 6 F and G) we assumed an indirect effect for instance by EVT-CM-driven induction of IL-10, as

422 previously shown for cancer-derived PD-L1 (22) or by other TGFβ-driven effects on
423 decPAMs. However, EVT-CM neither altered IL-10 secretion by cultivated decPAMs nor did
424 TGFβ blockage alter the suppressive effect of EVT-CM on decPAM-induced T cell
425 proliferation (Fig. 6, G and H). Lastly, we incubated decP explant tissues with EVT-CM and
426 found significantly induced EdU incorporation into macrophages when compared to control
427 treatment. In this setting, the addition of a neutralizing antibody against TGFβ reversed the
428 growth-promoting effect of EVT-CM (Fig. 6 I).
429 In summary, these data show that EVTs have the capacity to trigger a pregnancy-tolerant
430 phenotype in macrophages via their pleiotropically acting secreted factors.
431

432 **Discussion**

433 In this study, we describe profound phenotypical and functional differences of tissue-resident
434 macrophages in dependence on their localization within the human decidua. We established
435 a donor-matched cohort including well-characterized decB and decP tissue samples and
436 developed a flow cytometry panel to dissect tissue-resident macrophages from monocytes.
437 Interestingly, a computational comparison of our bulk RNA-seq analysis with published
438 scRNA-seq data revealed that the transcriptomes of decBAMs and decPAMs have significant
439 overlaps to the recently identified dM1 and dM2 subtypes, respectively. The substantial
440 difference between decBAMs and decPAMs in terms of transcripts, cellular proteome, and
441 secretome also translated into different functional phenotypes. While decBAMs are likely
442 replenished by local proliferation, induce Treg formation, and secrete important pregnancy-
443 sustaining factors such as IL-10, decPAMs exhibit a more motile phenotype with higher
444 efficiency to phagocytose and to trigger T cell proliferation. Finally, we show that EVT-CM re-
445 programs decPAMs into a functional phenotype, reminiscent of decBAMs.

446 During the first trimester of pregnancy, blastocyst implantation and subsequent formation of
447 the embryo and placenta do not affect the entire decidua. We therefore hypothesized that
448 maternal immunological adaptation in the decidua is differentially regulated depending on the
449 site of placentation. Indeed, our flow cytometry approach revealed significant differences by
450 identifying a decB-associated increase in neutrophil and macrophage accumulation. In
451 addition, we refined the previously reported pregnancy-dependent increase in dNK cells by
452 showing that this phenomenon is particularly pronounced in decP rather than the maternal-
453 fetal interface. While decB constitutes the actual maternal-fetal interface, decP areas make
454 up by far the largest part of the pregnant uterus in the first trimester. It may therefore easily
455 be possible that previous studies on dNK cell distribution in the first trimester of pregnancy
456 were compromised by decP tissue contamination.

457 Due to the lack of suitable cell surface markers, we sought to establish a gating strategy
458 allowing us to distinguish true tissue macrophages from other blood or tissue-derived
459 myeloid cell types including monocytes and DCs. This issue was particularly relevant for our

460 study as known markers to distinguish human APC-like myeloid populations in understudied
461 tissues such as the decidua are scarce. Owing to the high vascularization of the decidua,
462 distribution of specific immune cells within enzymatic decidua tissue digests is often
463 compared with those in peripheral blood in order to assess local accumulation of cells. This
464 approach, however, bears relevant caveats. Firstly, this method does not take into account
465 that immune cell distributions differ between peripheral blood and tissue capillaries. For
466 instance, it has been shown that intravascular T cells accumulate in the lumen of decidual
467 vessels by adhering to vessels but do not infiltrate the tissue (8). Secondly, so-called non-
468 classical monocytes have been described to accumulate at specific sites adhering to the
469 vascular wall (23) and, under specific conditions, are also able to infiltrate the tissue without
470 differentiating into macrophages (24, 25). Therefore, we established a novel gating strategy,
471 allowing us to specifically distinguish tissue macrophages from blood- or vessel-associated
472 monocytes. Indeed, $CD14^{+}CD163^{-}CD206^{-}$ cells clearly differ from decidual tissue-resident
473 macrophages and show upregulation of typical blood monocyte markers including the
474 prototypical blood-associated immune cell marker L-selectin (*SELL*). Further immunotyping
475 of $CD14^{+}CD163^{+}CD206^{+}$ decidual macrophages revealed high expression of lineage-
476 associated hallmark genes such as *MERTK* or *MAFB* and induction of other typical markers
477 for human and mouse macrophages, including *CD14*, *CD68*, *CEBPD*, *FCGR1A* (CD64) or
478 *FCGR2A* (CD32) (15). In addition, we find that these cells show typical macrophage
479 morphology, high autofluorescence and side scatter as well as absence of typical DC-
480 associated lineage markers such as *CD1A*/*B*/*C*, *CD226*, *FLT3* or *KIT* (14, 16, 17). These
481 data indicate that $CD14^{+}CD163^{+}CD206^{+}$ cells represent true tissue-resident decidual
482 macrophages.
483 We identified over 500 DEGs to be overexpressed in decBAMs when compared to decPAMs,
484 and subsequent enrichment analysis indicated them to be associated with neutrophil and
485 myeloid cell activation. Well in line, isolated and short-term cultivated decBAMs actively
486 secrete high levels of CXCL1, CXCL5, CXCL8, IL-10, and M-CSF. The latter two in
487 particular, have been shown to exert crucial functions during pregnancy for instance by

488 inducing a decidual-like phenotype in monocyte-derived macrophages (26-28) thereby acting
489 in an autocrine self-perpetuating manner. Furthermore, reduced IL-10 blood levels are
490 associated with human pregnancy disorders such as preeclampsia (29) and while
491 administration of IL-10 prevents naturally occurring fetal losses (30), its deletion can provoke
492 spontaneous abortions in mice (31). M-CSF has been shown to support placental function by
493 affecting EVT invasion (32). In addition, we find that decBAMs overexpress specific cell
494 surface markers including CD11c allowing for flow cytometry-based separation of decBAMs
495 and decPAMs in non-characterized decidual tissues. Indeed, CD11c has previously been
496 suggested to distinguish different decidual macrophage populations (27, 33), however not in
497 the context of differences between decB and decP areas. Along these lines, our comparative
498 computational approach demonstrated that our decBAM and decPAM populations share
499 major similarities with dM1 and dM2 populations identified by scRNA-seq (9), respectively.
500 This implies that the previously suggested macrophage heterogeneity at the maternal-fetal
501 interface is likely a consequence of not considering decP contamination, which we excluded
502 by a thorough patient-matched tissue sampling strategy.
503 Further comparative studies revealed a significant difference in the expression of HLA class
504 II molecules in $CD14^+$ tissue macrophages of decB and decP tissue samples. This
505 observation correlated with a higher transcript level of specific HLA class II molecules in
506 decPAMs. Functional assays revealed that decPAMs are efficient phagocytes, stimulate T
507 cell proliferation and show a migratory phenotype. These data imply that decPAMs constitute
508 the major tissue-resident APC population, where they serve as patrolling cells to protect the
509 maternal-fetal interface from invading pathogens. However, migratory APCs are central in
510 priming T cell responses to peripheral tissue antigens (34, 35) and thus pose a critical threat
511 to human pregnancy by potentially triggering T cell responses to placental antigens. Indeed,
512 decBAMs are significantly impaired in their migratory and phagocytic activity as well as in
513 their potential to trigger T cell proliferation. In line with this, decBAMs induced higher
514 numbers of $CD4^+CD25^+FOXP3^+$ Tregs. This phenomenon is well-described for IL10- and
515 TGFβ-secreting anti-inflammatory macrophages (36) and has also been assigned to decidual

516 macrophages (21), however not in comparison to decPAMs. Accumulatively, our descriptive
517 and functional data imply that decBAMs trigger a broad anti-inflammatory environment
518 towards T cell activation and are likely one of the main inducers of neutrophil influx. Indeed,
519 neutrophils are specifically attracted by decB-CM, which was shown to be rich in decBAM-
520 secreted neutrophil chemoattractants including CXCL1, CXCL8, and CXCL5. So-called
521 myeloid-derived suppressor cells (MDSCs), shown to inhibit $CD8^+$ T cell function accumulate
522 in the blood of pregnant women (37) and were also reported to accumulate in the decidua
523 (38). Well in line, we find that decB-derived neutrophils secrete high levels of MMP-9 and the
524 neutrophil-associated chemokines S100A8 and S100A9. While the latter two have recently
525 been suggested to serve as markers for MDSCs (39), MMP-9 production is also a feature of
526 tumor-associated neutrophils and was found to trigger tissue remodeling and angiogenesis in
527 this context (40, 41).
528 Maintenance of tissue macrophages can be regulated via two different routes. Originally,
529 macrophages are described to differentiate from infiltrating bone marrow-derived circulating
530 monocytes (42). Pioneering work in mice however, showed that macrophages are also
531 replenished by locally proliferating, so-called tissue resident macrophages (43). In mice, self-
532 renewing yolk sac-derived macrophages are seeded into tissues during development where
533 they expand during embryonic development and reside throughout adult life (43, 44). While
534 local renewal of human tissue macrophages, independent of blood monocyte influx, has
535 been confirmed in various transplantation studies in the liver (45), brain (46), lung (47, 48)
536 and heart (49), a definitive proof for the existence of long-lived yolk sac-derived, tissue-
537 resident macrophages in humans is missing. In our study we find that decBAMs show signs
538 for DNA synthesis in an *ex vivo* assay and a higher proliferative capacity *in situ*, compared to
539 decPAMs. Although we cannot exclude macrophage replenishment by monocyte
540 extravasation, additional *ex vivo* assays suggest that decB-CMs do not exert higher potential
541 to attract monocytes when compared to decP explant-CMs. Macrophage proliferation at the
542 maternal fetal interface has further been confirmed in Hofbauer cells, which likely replenish
543 independently of the embryonic bone marrow as they locally proliferate and share

544 transcriptional overlap with human yolk sac macrophages but not embryonic monocytes (10).
545 However, tissue resident macrophage biology is greatly dependent on extrinsic stimuli
546 suggesting that the local environment determines the mature functionality of macrophages
547 (43). For instance, macrophage progenitors, regardless of ontogeny, equally develop into
548 fully functional alveolar macrophages (50) and peritoneal macrophage diversity was shown
549 to be determined by tissue-derived signals rather than intrinsic factors (51). We therefore
550 tested whether the specific decBAM phenotype is controlled by extrinsic factors such as
551 placenta-derived signals.
552 To test this hypothesis, we incubated isolated decPAMs with CM of cultivated primary EVTs
553 in order to mimic trophoblast-dependent effects on decidual macrophages, unaffected by
554 placentation *in utero*. Functional studies on viable tissue explants revealed that indeed
555 placenta-derived signals can override the tissue-specific phenotype of decPAMs. In this
556 setting, the addition of EVT-CM led to a significant induction of proliferation and upregulation
557 of CD44 expression, a marker of decBAMs. Paralleling the phenomenon observed in decP
558 tissue explants, EVT-CM also changed the functionality of isolated decPAMs by suppressing
559 their migratory and phagocytic activity. Similar observations have been made in cancer
560 where tumor cells selectively inhibit phagocytosis of tumor-associated macrophages (TAMs)
561 supposedly to avoid generation of tumor antigen-specific cytotoxic T cells (52). Indeed,
562 restoration of the phagocytic activity in TAMs led to cancer-specific priming of $CD8^+$ T cells
563 (53). Similar to the reduced ability of decBAMs to trigger T cell proliferation, decPAM-
564 mediated T cell activation was also significantly suppressed upon addition of EVT-CM. These
565 data show that EVT-derived factors indeed play a central role in the extrinsic control of
566 macrophage function. Neutralizing antibodies targeting TGFβ, PD-L1 or IL-10 had no effect
567 on the EVT-CM dependent effects on decPAM. This is likely due to the pleiotropic effect of
568 EVT-CM on decidual macrophages also noticed by another study reporting that the $FOXP3^+$
569 Treg-inducing effect of EVTs was unaffected by the addition of neutralizing antibodies
570 targeting CD3, HLA-C, HLA-G, ILT2, TGFβ and PD-L1 (21). However, selective blockage of
571 TGFβ reversed the growth-promoting effect of EVT-CM in decPAMs. This observation

572 together with our finding that isolated decBAMs secrete high levels of M-CSF implies a
573 growth-inducing autocrine loop as well as extrinsic proliferative stimuli by invasive EVTs.
574 Indeed, TGFβ1 has been shown to enhance macrophage proliferation via the induction of M-
575 CSF (54).
576 The generation of an immunosuppressive environment is decisive for a successful
577 pregnancy. However, our data impose that this phenomenon does not affect the entire
578 decidua. In fact, we find that macrophages further away from the placentation site, referred to
579 as decPAM in this study, show functionality of tissue-patrolling macrophages. In contrast,
580 decBAMs residing at the maternal-fetal interface exhibit significantly less pronounced APC-
581 like function. Our study further implies that this pregnancy tolerant phenotype is dictated by
582 the placenta as EVTs can be used to re-program decPAMs towards a state reminiscent of
583 decBAMs.
584

585 **Material and Methods**

586

587 **Ethical considerations**

588 All experiments and analyses were conducted in accordance with the Declaration of Helsinki
589 as well as Austrian laws and guidelines. First trimester (6 – 10 weeks of gestation, n = 97)
590 decidual and placental tissues were derived from women undergoing elective termination of
591 pregnancy for nonmedical reasons. The use of patient material was approved by the Ethics
592 Committee of the Medical University of Vienna. Ethical approvals are annually renewed. The
593 use of blood samples from healthy control women for migration assays of PBMCs was
594 approved by the Regional Ethics Committee in Linköping, Sweden. Written informed consent
595 was obtained from all subjects.

596
597 **Cell isolation**

598 For decidual and endometrial immune cell isolation, tissue was cut into small pieces using a
599 scalpel and digested using 2,5 µg/ml Collagenase IV (Worthington) and 25 mg/ml DNase I
600 (Sigma-Aldrich) with the 37°C Multi-B program of a gentleMACS Dissociator (Miltenyi
601 Biotec). The resulting single cell suspension was passed through a 70 µm cell strainer
602 (Falcon). If necessary, red blood cells were lysed by incubating cells in a buffer containing
603 155 mM NH4Cl, 10 mM KHCO3, and 0.1 mM EDTA (pH 7.3) for 5 min, before staining for
604 flow cytometry or sorting.

605 For flow cytometry and sorting, macrophages were defined as $CD45^{+}CD14^{+}CD163^{+}CD206^{+}$,
606 monocytes were defined as $CD45^{+}CD14^{+}CD163^{-}CD206^{-}$, and neutrophils were defined as
607 CD45+CD66b+. Dead cells were excluded using the viability dye Zombie Violet (BioLegend).
608 For generation of conditioned media, sorted cells were seeded onto Nunc Cell-Culture plates
609 (ThermoFisher) at a density of 1 million cells/ml in Decidua culture medium, consisting of
610 DMEM/F-12 without phenol red (Gibco), supplemented with 10% FBS superior (Sigma
611 Aldrich), 50 µg/ml gentamicin (Gibco) and ITS+ Premix (Corning), and cultured for 20 hours
612 at 37°C. Cell culture supernatants were then centrifuged at 12000 g for 10 minutes at 4°C,
613 snap frozen in liquid nitrogen, and stored at -80°C until further use.

614 PAMMs were isolated according to a published protocol (10), with some adjustments. Briefly,
615 villi were scraped with a scalpel and digested with 0.2% Trypsin (Invitrogen) and 12.5 mg/ml
616 DNase I (Sigma-Aldrich) in HBSS-Mg/Ca-free medium (Sigma-Aldrich) at 37°C for 7 min.
617 The resulting single cell suspension was passed through a 70 µm cell strainer (Falcon). If
618 necessary, red blood cells were lysed by incubating cells in a buffer containing 155 mM
619 NH4Cl, 10 mM KHCO3, and 0.1 mM EDTA (pH 7.3) for 5 min, before staining for FACS
620 sorting. PAMMs were defined as CD45+HLA-DR+ cells.
621 Primary EVTs were isolated according to a previously published protocol (55). Briefly, villi
622 were scraped with a scalpel and digested in two sequential digestion steps using 0.125%
623 trypsin (Invitrogen) and 12.5 mg/ml DNase I (Sigma-Aldrich) in HBSS-Mg/Ca-free medium
624 (Sigma-Aldrich). Each digest was performed at 37°C for 30 min without agitation.
625 Subsequently, cells were filtered through a 100 µm cell strainer (Falcon). The cells were then
626 layered on top of a Percoll gradient (10–70%; Pharmacia, Uppsala, Sweden) and centrifuged
627 at 1,175 g at 4°C for 24 min without braking at the end of the run. Cells between 35% and
628 50% of the Percoll layer were collected. If necessary, red blood cells were lysed by
629 incubating cells in a buffer containing 155 mM NH4Cl, 10 mM KHCO3, and 0.1 mM EDTA
630 (pH 7.3) for 5 min.
631 Remaining cells were then magnetically labeled with HLA-G – PE antibody and anti-PE
632 microbeads and enriched for HLA-G+ EVTs by magnetic-activated cell sorting using an
633 OctoMACS separator and MS columns (Miltenyi Biotec).
634 HLA-G+ EVTs were seeded on fibronectin-coated tissue culture plates (Nunc Cell-Culture
635 Plates, ThermoFisher) at a density of 1 million cells/ml EVT culture medium, consisting of
636 DMEM/F-12, GlutaMAX (Gibco), supplemented with 10% FBS Superior (Sigma Aldrich), 50
637 µg/ml gentamicin (Gibco), and 0.5 µg/mL fungizone (Gibco), and left to differentiate for 1-3
638 days before collecting cell culture supernatants. The conditioned media were centrifuged at
639 12000 g for 10 minutes at 4°C, snap frozen in liquid nitrogen, and stored at -80°C until further
640 use.
641
642

643 **Cell density**

644 To determine the density of cells within decidual tissues, the tissue was weighed before
645 digestion and the weight was correlated with the cellular output after digestion, determined
646 by a CASY TT cell counter.

647

648 **Flow cytometry**

649 For analysis of immune cell distributions within decidual and endometrial tissues, cells were
650 isolated as described above and stained for flow cytometry using the antibodies listed in
651 Table S1. Immune cells were defined as $CD45^{+}$. Within the immune cell gate, neutrophils
652 were defined as $CD66b^{+}$, macrophages/monocytes were defined as $CD66b^{-}CD14^{+}$, dNK/uNK
653 cells were defined as $CD3^{-}CD56^{hi}$, T cells were defined as $CD3^{+}$, and B cells were defined as
654 $CD19^{+}$. All defined immune cell types were mutually exclusive.

655 To create the TSNE plot in Fig. 1 we used the CyTOF workflow as published by Nowicka et
656 al. (56) and modified it accordingly for flow cytometry data.

657

658 **Immunofluorescence of decidual tissue sections**

659 First trimester decidual tissues were fixed in 7.5% formaldehyde and embedded in paraffin
660 (Merck). Sections (2.5 µm) were cut using a microtome (HM355; Microm) and deparaffinized
661 by incubating for 10 minutes in Xylene, followed by 100%, 96%, and 70% ethanol, and
662 deionized water. Antigens were retrieved using citrate buffer (pH 6.0, Sigma-Aldrich) in a
663 KOS MicrowaveStation (Milestone SRL).

664 For staining, sections were blocked for 1 hour in TBS/T containing 5% normal goat serum
665 (Cell Signaling Technology) and then incubated with primary antibodies listed in Table S1
666 overnight at 4°C. Subsequently, the slides were washed in TBS/T 3 times and then incubated
667 with secondary antibodies (2 µg/ml) and DAPI (1 µg/ml, Roche) for 1 hour at room
668 temperature.

669 Images were acquired on a fluorescence microscope (Olympus BX50) using a Hamamatsu
670 ORCA-sparc digital camera and the Olympus cellSens Standard software.

671 **Explant culture**

672 Explants were generated by cutting decB and decP tissue into small pieces of approximately
673 1x1 cm. Explants were weighed and put into 4 ml of Decidua culture medium per 1 gram of
674 tissue, then cultured overnight at 37°C. Conditioned media were centrifuged at 12000 g for
675 10 minutes at 4°C, snap frozen in liquid nitrogen and stored at -80°C until further use.
676 To assess the effect of EVT-CM on macrophages *in situ*, explants were cultured in 50%
677 EVT-CM overnight, then fixed in 7.5% formaldehyde and processed for immunofluorescence
678 as described above. For proliferation assays, 10 µM EdU (EdU-Click 488 kit, baseclick) was
679 added to the explant culture and the EdU detection protocol was performed according to
680 manufacturer's user manual before blocking. Sections were co-stained with CD14, and
681 macrophage EdU incorporation was assessed using the ImageJ software.
682 For blockage experiments, 1 µg/ml anti-human TGF-β antibody was added to the culture.
683

684 **Analysis of conditioned media**

685 Conditioned media from decB and decP explants were analyzed by the proximity extension
686 assay on the Olink proteomics platform (www.olink.com), using the Inflammation Panel.
687 Samples were sent to and analyzed by the Clinical Biomarker Facility Unit at SciLifeLab in
688 Uppsala, Sweden.
689 Conditioned media from decB and decP explants, as well as decBAMMs, decPAMMs, EVTs,
690 and decB neutrophils, were analyzed using the magnetic bead-based immunoassays by Bio-
691 Techne (Luminex Performance Assay TGF-β Premixed Kit and Luminex Discovery Assay
692 with personalized panels). The samples were processed according to manufacturer's user
693 manual and measured on a Luminex 200 machine.
694

695 **RNA sequencing**

696 After isolation of macrophages or monocytes (as described above), RNA was extracted using
697 the SPLIT RNA Extraction Kit (Lexogen) and sent to Lexogen in Vienna for library
698 preparation and sequencing (QuantSeq). Fastq files were aligned to the human reference

genome GRCh38 with Gencode annotation using STAR aligner in 2-pass mode (57). The count matrices were calculated with STAR/htseq-count. Differential gene expression was calculated using DESeq2 (58) , applying batch modelling where required. Genes with counts lower than 100 in 90% of samples were filtered out. LFC shrinkage with approximate posterior estimation for GLM coefficients was applied for downstream visualization (59) . For the PCA visualization, batch effects were removed with limma (60). We calculated Gene Ontology enrichment scores with the webtool g:Profiler and plotted the data in R (61-63).

scRNA-seq data were downloaded from EMBL-EBI using the accession number E-MTAB-6701. Raw sequencing data were aligned to the reference genome GRCh38 using 10x Genomics Cell Ranger 6.1.2. Output files were analyzed and filtered with the R package Seurat 4.0.6 (64-67). All cells with low overall gene expression or which showed high mitochondrial gene expression were filtered out. The data were log-normalized before entering the Seurat integration workflow. Cluster annotation was performed applying the list of cluster-specific genes published along with the original publication (9). Violin plots were created with the Seurat VInplot function, using either single gene expression or module scores, calculated with the Seurat AddModuleScore function (64-67).

PBMC migration assay

Blood from healthy, non-pregnant female donors was collected in Na-heparin tubes and PBMCs were isolated using Lymphoprep (Axis Shield) according to manufacturer's instruction. Conditioned media of decB and decP explants were pipetted into wells of a 24-well plate (Corning) at a concentration of 25% CM in Transwell medium consisting of Roswell Park Memorial Institute (RPMI) 1640 medium supplemented with 1 mg/ml human serum albumin (Octapharma), and 100 units/ml penicillin, 100 µg/ml streptomycin and 29.2 mg/ml L-glutamine (Gibco). Transwell inserts (6.5 mm inserts with 5.0 µm pores, Corning) were coated with 1.43 mg/ml Matrigel (Growth factor-reduced, Corning) for 1 hour at room temperature. Then, the inserts were placed into the wells containing the CM and the plate was pre-incubated for 1 hour at 37°C. PBMCs were seeded into the top part of the transwell

727 insert (0.5 million cells in 100 µl Transwell medium) and the plate was incubated at 37°C for
728 4 hours. Migrated cells were collected by taking up the medium from the bottom part of the
729 transwell and scraping any adherent cells off the bottom of the plate. Cells were then stained
730 for flow cytometry and analyzed using a FACSCanto II flow cytometer (BD). TruCount tubes
731 (BD) were used to determine the absolute numbers of migrated cells.
732

733 **Neutrophil migration assay**

734 Neutrophil migration towards decB and decP supernatants was measured using 96-well
735 trans well plates (Corning, 5 µm polycarbonate membranes). Filters were pre-soaked in
736 buffer (PBS with Ca2+/Mg2+ supplemented with 0.1% BSA, 10 mM HEPES, and 10 mM
737 glucose) for 1 hr at 37°C. Polymorphonuclear leukocytes (PMNLs) were isolated from
738 healthy, non-pregnant donors as previously described (68). Bottom wells were loaded with
739 100 µl supernatants (1:2 dilution with media) and upper wells with 100 µl PMNL (4x106
740 cell/ml). Cells were allowed to migrate for 1hr at 37°C and subsequently fixed with 150 µl of
741 fixation solution (CellFIX, BD). Number of migrated neutrophils was measured at a BD
742 FACSCanto II for 30 sec and separated from eosinophils based on their different auto-
743 fluorescence in the V450 channel.
744

745 **Cell Tracking**

746 For in vitro analysis of cell motility, macrophages were seeded at a density of 250.000
747 cells/ml Decidua culture medium and incubated in a Lionheart FX automated live cell imager
748 at 37°C and 5% CO2. Time-lapse videos were created by taking a picture every 5 minutes
749 for 24 hours, using the Gen5 3.08 software. All images between 12 and 24 hours of culture
750 were used to track cells and analyze their speed with the CellTracker tool in MATLAB
751 (http://celltracker.website). Cell starting coordinates were set to 0,0 and subsequent data
752 points were newly calculated accordingly for visualization purposes. Cell tracks were
753 visualized in R.
754

755 **Phagocytosis Assay**

756 Decidual cells were isolated as described above and incubated in the presence of
757 fluorescence-labeled latex beads (50 beads per cell; latex beads, 1 µm, carboxylate-modified
758 polystyrene, fluorescent yellow-green, Merck) for 2 hours at 37°C. A negative control was
759 incubated for 2 hours at 4°C to control for non-specific adhesion of beads to the cell surface.
760 Then, cells were detached from the plate using Accutase (Gibco StemPro Accutase, Fisher
761 Scientific) and stained for flow cytometry. Phagocytosis was assessed on a FACSVerse flow
762 cytometer using the BD FACSuite software, by measuring the signal of the beads within the
763 macrophage gate (using the negative control as a gate-setting control).
764 To measure the effect of EVT-CM on macrophage phagocytosis, the cells were cultured in
765 50% EVT-CM. For blockage experiments, 1 µg/ml anti-human TGF-β or 20 µg/ml anti-human
766 PD-L1 antibody was added to the culture.
767

768 **T cell assays**

769 T cells were isolated from PBMC of healthy, non-pregnant female volunteers using the Pan T
770 Cell Isolation Kit (Miltenyi,130-096-535). To monitor proliferation, T cells were labeled with 5
771 µM carboxyfluorescein diacetate succinimidyl (CFSE Cell Division Tracker Kit, Biolegend).
772 For Treg induction and T cell activation, flat-bottomed 96-well plates (Nunc Cell-Culture
773 Plates, ThermoFisher) were coated with 1 µg/ml anti-CD3 and 2 µg/ml anti-CD28 antibodies
774 (BioLegend) for 2 hours and seeded with 50.000 T cells/well. To measure the effect of
775 macrophages and EVT-CM on T cell proliferation and Treg induction, 5.000 macrophages
776 and/or 50% EVT-CM were added to the culture. For the blockage experiments, 1 µg/ml anti-
777 human TGF-β antibody was added to the co-culture. After three days, T cell proliferation was
778 determined by CFSE dilution and Treg differentiation was determined by surface staining of
779 CD25 and intracellular staining of FOXP3 using the eBioscience Foxp3/Transcription Factor
780 staining buffer set (Invitrogen). Data were collected using a FACSVerse flow cytometer using
781 the BD FACSuite software and were analyzed with FlowJo 10.7.
782

783 **Accession codes and data availability**

784 BioProject accession number for RNA-seq of isolated samples: GSE196917

785

786 **Acknowledgments**

787 We thank all patients and staff at Gynmed Clinic (Vienna) for providing placental and
788 decidual samples. We thank the FACS Core Unit at the St. Anna Children's Cancer
789 Research Institute (Vienna) and Boris Kovacic and Dieter Printz (St. Anna Children's Cancer
790 Research Institute Vienna) are greatly acknowledged for technical help and advices with flow
791 cytometry-based analysis and sorting. Emir Hadzijusufovic (Division of Hematology and
792 Hemostaseology, Department of Internal Medicine I, Medical University of Vienna) is
793 acknowledged for technical help with cell staining. The authors would like to acknowledge
794 support of the Clinical biomarker facility at SciLifeLab Sweden for providing assistance in
795 protein analyses. We thank Benjamin Schuster (Vienna University of Technology) for his help
796 with computational analysis. Thomas Weichhart (Center of Pathobiochemistry and Genetics,
797 Institute of Medical Genetics, Medical University of Vienna, Vienna) is acknowledged for
798 scientific discussion.
799 This work was supported by the Austrian Science Fund (P33485 to J.P.) and by the Austrian
800 National Bank (17613ONB to J.P.).

801

802 **Author contributions**

803 Conceptualization, J. Pollheimer, S. Vondra, A.L. Höbler, A.I. Lackner, R. Bauer, J. Kargl, J.
804 Ernerudh. Formal analysis, J. Pollheimer, S. Vondra, A.L. Höbler, A.I. Lackner, J.
805 Raffetseder, Z.N. Mihalic, V. Kunihs, P. Haslinger, S. Haider, J. Kargl, H. Husslein. Funding
806 acquisition, J. Pollheimer. Methodology, J. Pollheimer, S. Vondra, A.L. Höbler, A.I. Lackner,
807 J. Raffetseder, S. Haider, R. Oberle, M. Wahrmann, J. Ernerudh, J. Kargl. Intellectual input,
808 J. Pollheimer, S. Vondra, A.L. Höbler, A.I. Lackner, J. Raffetseder, L. Saleh, S. Haider, M.
809 Wahrmann, R. Bauer, J. Kargl, H. Husslein, P. Latos, M. Knöfler, J. Ernerudh. Supervision, J.

Pollheimer. Visualization, J. Pollheimer, S. Vondra, A.L. Höbler, A.I. Lackner. Writing, J. Pollheimer, S. Vondra, A.L. Höbler, A.I. Lackner.

All authors discussed the manuscript.

Competing Interests

Disclosures: The authors declare no competing interests exist.

References

1. Knofler M, *et al.* (2019) Human placenta and trophoblast development: key molecular mechanisms and model systems. *Cell Mol Life Sci* 76(18):3479-3496.
2. Brosens I, Pijnenborg R, Vercruysse L, & Romero R (2011) The "Great Obstetrical Syndromes" are associated with disorders of deep placentation. *Am J Obstet Gynecol* 204(3):193-201.
3. Erlebacher A (2013) Immunology of the maternal-fetal interface. *Annu Rev Immunol* 31:387-411.
4. Moffett A, Chazara O, & Colucci F (2017) Maternal allo-recognition of the fetus. *Fertil Steril* 107(6):1269-1272.
5. Pollheimer J, Vondra S, Baltayeva J, Beristain AG, & Knofler M (2018) Regulation of Placental Extravillous Trophoblasts by the Maternal Uterine Environment. *Front Immunol* 9:2597.
6. Gamliel M, *et al.* (2018) Trained Memory of Human Uterine NK Cells Enhances Their Function in Subsequent Pregnancies. *Immunity* 48(5):951-962 e955.
7. Tilburgs T, Evans JH, Crespo AC, & Strominger JL (2015) The HLA-G cycle provides for both NK tolerance and immunity at the maternal-fetal interface. *Proc Natl Acad Sci U S A* 112(43):13312-13317.
8. Nancy P, *et al.* (2012) Chemokine gene silencing in decidual stromal cells limits T cell access to the maternal-fetal interface. *Science* 336(6086):1317-1321.
9. Vento-Tormo R, *et al.* (2018) Single-cell reconstruction of the early maternal-fetal interface in humans. *Nature* 563(7731):347-353.
10. Thomas JR, *et al.* (2021) Phenotypic and functional characterization of first-trimester human placental macrophages, Hofbauer cells. *J Exp Med* 218(1).
11. Plaisier M, *et al.* (2007) Different degrees of vascularization and their relationship to the expression of vascular endothelial growth factor, placental growth factor, angiopoietins, and their receptors in first-trimester decidual tissues. *Fertil Steril* 88(1):176-187.
12. Windsperger K, *et al.* (2020) Densities of decidual high endothelial venules correlate with T-cell influx in healthy pregnancies and idiopathic recurrent pregnancy losses. *Hum Reprod* 35(11):2467-2477.
13. Abbas Y, *et al.* (2019) Tissue stiffness at the human maternal-fetal interface. *Hum Reprod* 34(10):1999-2008.
14. McGovern N, *et al.* (2014) Human dermal CD14(+) cells are a transient population of monocyte-derived macrophages. *Immunity* 41(3):465-477.
15. Xue J, *et al.* (2014) Transcriptome-based network analysis reveals a spectrum model of human macrophage activation. *Immunity* 40(2):274-288.
16. Gautier EL, *et al.* (2012) Gene-expression profiles and transcriptional regulatory pathways that underlie the identity and diversity of mouse tissue macrophages. *Nat Immunol* 13(11):1118-1128.
17. Tamoutounour S, *et al.* (2013) Origins and functional specialization of macrophages and of conventional and monocyte-derived dendritic cells in mouse skin. *Immunity* 39(5):925-938.
18. Kolaczkowska E & Kubes P (2013) Neutrophil recruitment and function in health and inflammation. *Nat Rev Immunol* 13(3):159-175.
19. Zenz R, *et al.* (2005) Psoriasis-like skin disease and arthritis caused by inducible epidermal deletion of Jun proteins. *Nature* 437(7057):369-375.
20. Fan X, *et al.* (2014) Endometrial VEGF induces placental sFLT1 and leads to pregnancy complications. *J Clin Invest* 124(11):4941-4952.
21. Salvany-Celades M, *et al.* (2019) Three Types of Functional Regulatory T Cells Control T Cell Responses at the Human Maternal-Fetal Interface. *Cell Rep* 27(9):2537-2547 e2535.
22. Gordon SR, *et al.* (2017) PD-1 expression by tumour-associated macrophages inhibits phagocytosis and tumour immunity. *Nature* 545(7655):495-499.
23. Thomas G, Tacke R, Hedrick CC, & Hanna RN (2015) Nonclassical patrolling monocyte function in the vasculature. *Arterioscler Thromb Vasc Biol* 35(6):1306-1316.
24. Jakubzick C, *et al.* (2013) Minimal differentiation of classical monocytes as they survey steady-state tissues and transport antigen to lymph nodes. *Immunity* 39(3):599-610.
25. Rodero MP, *et al.* (2015) Immune surveillance of the lung by migrating tissue monocytes. *Elife* 4:e07847.
26. Lindau R, *et al.* (2021) Decidual stromal cells support tolerance at the human foetal-maternal interface by inducing regulatory M2 macrophages and regulatory T-cells. *J Reprod Immunol* 146:103330.
27. Svensson J, *et al.* (2011) Macrophages at the fetal-maternal interface express markers of alternative activation and are induced by M-CSF and IL-10. *J Immunol* 187(7):3671-3682.
28. Svensson-Arvelund J, *et al.* (2015) The human fetal placenta promotes tolerance against the semiallogeneic fetus by inducing regulatory T cells and homeostatic M2 macrophages. *J Immunol* 194(4):1534-1544.

29. Nath MC, Cubro H, McCormick DJ, Milic NM, & Garovic VD (2020) Preeclamptic Women Have Decreased Circulating IL-10 (Interleukin-10) Values at the Time of Preeclampsia Diagnosis: Systematic Review and Meta-Analysis. *Hypertension* 76(6):1817-1827.
30. Chaouat G*, et al.* (1995) IL-10 prevents naturally occurring fetal loss in the CBA x DBA/2 mating combination, and local defect in IL-10 production in this abortion-prone combination is corrected by in vivo injection of IFN-tau. *J Immunol* 154(9):4261-4268.
31. Murphy SP, Fast LD, Hanna NN, & Sharma S (2005) Uterine NK cells mediate inflammation-induced fetal demise in IL-10-null mice. *J Immunol* 175(6):4084-4090.
32. Hamilton GS, Lysiak JJ, Watson AJ, & Lala PK (1998) Effects of colony stimulating factor-1 on human extravillous trophoblast growth and invasion. *J Endocrinol* 159(1):69-77.
33. Houser BL, Tilburgs T, Hill J, Nicotra ML, & Strominger JL (2011) Two unique human decidual macrophage populations. *J Immunol* 186(4):2633-2642.
34. Allenspach EJ, Lemos MP, Porrett PM, Turka LA, & Laufer TM (2008) Migratory and lymphoid-resident dendritic cells cooperate to efficiently prime naive CD4 T cells. *Immunity* 29(5):795-806.
35. Itano AA*, et al.* (2003) Distinct dendritic cell populations sequentially present antigen to CD4 T cells and stimulate different aspects of cell-mediated immunity. *Immunity* 19(1):47-57.
36. Ruffell B & Coussens LM (2015) Macrophages and therapeutic resistance in cancer. *Cancer Cell* 27(4):462-472.
37. Kostlin N*, et al.* (2014) Granulocytic myeloid derived suppressor cells expand in human pregnancy and modulate T-cell responses. *Eur J Immunol* 44(9):2582-2591.
38. Kang X*, et al.* (2016) Granulocytic myeloid-derived suppressor cells maintain feto-maternal tolerance by inducing Foxp3 expression in CD4+CD25-T cells by activation of the TGF-beta/beta-catenin pathway. *Mol Hum Reprod* 22(7):499-511.
39. Bronte V*, et al.* (2016) Recommendations for myeloid-derived suppressor cell nomenclature and characterization standards. *Nat Commun* 7:12150.
40. Ardi VC, Kupriyanova TA, Deryugina EI, & Quigley JP (2007) Human neutrophils uniquely release TIMP-free MMP-9 to provide a potent catalytic stimulator of angiogenesis. *Proc Natl Acad Sci U S A* 104(51):20262-20267.
41. Bekes EM*, et al.* (2011) Tumor-recruited neutrophils and neutrophil TIMP-free MMP-9 regulate coordinately the levels of tumor angiogenesis and efficiency of malignant cell intravasation. *Am J Pathol* 179(3):1455-1470.
42. van Furth R*, et al.* (1972) The mononuclear phagocyte system: a new classification of macrophages, monocytes, and their precursor cells. *Bull World Health Organ* 46(6):845-852.
43. Ginhoux F & Guilliams M (2016) Tissue-Resident Macrophage Ontogeny and Homeostasis. *Immunity* 44(3):439-449.
44. Palis J, Robertson S, Kennedy M, Wall C, & Keller G (1999) Development of erythroid and myeloid progenitors in the yolk sac and embryo proper of the mouse. *Development* 126(22):5073-5084.
45. Klein I*, et al.* (2007) Kupffer cell heterogeneity: functional properties of bone marrow derived and sessile hepatic macrophages. *Blood* 110(12):4077-4085.
46. Ginhoux F*, et al.* (2010) Fate mapping analysis reveals that adult microglia derive from primitive macrophages. *Science* 330(6005):841-845.
47. Bittmann I*, et al.* (2001) Cellular chimerism of the lung after transplantation. An interphase cytogenetic study. *Am J Clin Pathol* 115(4):525-533.
48. Byrne AJ*, et al.* (2020) Dynamics of human monocytes and airway macrophages during healthy aging and after transplant. *J Exp Med* 217(3).
49. Bajpai G*, et al.* (2018) The human heart contains distinct macrophage subsets with divergent origins and functions. *Nat Med* 24(8):1234-1245.
50. van de Laar L*, et al.* (2016) Yolk Sac Macrophages, Fetal Liver, and Adult Monocytes Can Colonize an Empty Niche and Develop into Functional Tissue-Resident Macrophages. *Immunity* 44(4):755-768.
51. Okabe Y & Medzhitov R (2014) Tissue-specific signals control reversible program of localization and functional polarization of macrophages. *Cell* 157(4):832-844.
52. Pathria P, Louis TL, & Varner JA (2019) Targeting Tumor-Associated Macrophages in Cancer. *Trends Immunol* 40(4):310-327.
53. Tseng D*, et al.* (2013) Anti-CD47 antibody-mediated phagocytosis of cancer by macrophages primes an effective antitumor T-cell response. *Proc Natl Acad Sci U S A* 110(27):11103-11108.
54. Celada A & Maki RA (1992) Transforming growth factor-beta enhances the M-CSF and GM-CSF-stimulated proliferation of macrophages. *J Immunol* 148(4):1102-1105.
55. Haider S*, et al.* (2016) Notch1 controls development of the extravillous trophoblast lineage in the human placenta. *Proc Natl Acad Sci U S A* 113(48):E7710-E7719.
56. Nowicka M*, et al.* (2017) CyTOF workflow: differential discovery in high-throughput high-dimensional cytometry datasets. *F1000Res* 6:748.
57. Dobin A*, et al.* (2013) STAR: ultrafast universal RNA-seq aligner. *Bioinformatics* 29(1):15-21.

938 58. Love MI, Huber W, & Anders S (2014) Moderated estimation of fold change and dispersion for RNA-
939 seq data with DESeq2. *Genome Biol* 15(12):550.
940 59. Zhu A, Ibrahim JG, & Love MI (2019) Heavy-tailed prior distributions for sequence count data:
941 removing the noise and preserving large differences. *Bioinformatics* 35(12):2084-2092.
942 60. Ritchie ME*, et al.* (2015) limma powers differential expression analyses for RNA-sequencing and
943 microarray studies. *Nucleic Acids Res* 43(7):e47.
944 61. Ashburner M*, et al.* (2000) Gene ontology: tool for the unification of biology. The Gene Ontology
945 Consortium. *Nat Genet* 25(1):25-29.
946 62. Gene Ontology C (2021) The Gene Ontology resource: enriching a GOld mine. *Nucleic Acids Res*
947 49(D1):D325-D334.
948 63. Reimand J, Kull M, Peterson H, Hansen J, & Vilo J (2007) g:Profiler--a web-based toolset for
949 functional profiling of gene lists from large-scale experiments. *Nucleic Acids Res* 35(Web Server
950 issue):W193-200.
951 64. Butler A, Hoffman P, Smibert P, Papalexi E, & Satija R (2018) Integrating single-cell transcriptomic
952 data across different conditions, technologies, and species. *Nat Biotechnol* 36(5):411-420.
953 65. Hao Y*, et al.* (2021) Integrated analysis of multimodal single-cell data. *Cell* 184(13):3573-3587 e3529.
954 66. Satija R, Farrell JA, Gennert D, Schier AF, & Regev A (2015) Spatial reconstruction of single-cell gene
955 expression data. *Nat Biotechnol* 33(5):495-502.
956 67. Stuart T*, et al.* (2019) Comprehensive Integration of Single-Cell Data. *Cell* 177(7):1888-1902 e1821.
957 68. Valadez-Cosmes P*, et al.* (2021) Identification of Novel Low-Density Neutrophil Markers Through
958 Unbiased High-Dimensional Flow Cytometry Screening in Non-Small Cell Lung Cancer Patients.
959 *Front Immunol* 12:703846.
960

961

962 **Supplementary Data**

963

964 **Fig. S1** presents a schematic illustrating how decidual samples were processed for
965 characterization and their cellular densities after enzymatic digestion. **Fig. S2** shows the
966 characterization of tissue-resident macrophages and presents the distribution of immune
967 cells in the secretory endometrium, decB, and decP samples. **Fig. S3** shows the data for
968 chemoattractant assays performed with decB- and decP-CMs using PBMCs. **Fig. S4**
969 represents PCA and gene set enrichment analysis of RNA-seq data and shows the
970 secretome of decidual explants and neutrophils. **Fig. S5** shows the capacity of EVT-CM-
971 treated decPAMs to induce Treg formation of isolated blood-derived T cells. **Data S1**
972 presents the complete list of measured factors by the Olink proteomics platform (related to
973 Fig. 1, D). **Table S1** provides a list of antibodies used in this study.

974

975

976

977

978

979

980

981

982

983